Development of Improved Materials for Environmental Applications: Nanocrystalline NaY Zeolites

ARTICLE *in* ENVIRONMENTAL SCIENCE AND TECHNOLOGY · APRIL 2005

Impact Factor: 5.33 · DOI: 10.1021/es049194z · Source: PubMed

4 AUTHORS, INCLUDING:

Gonghu Li
University of New Hampshire
39 PUBLICATIONS **1,731** CITATIONS

SEE PROFILE

Sarah C Larsen
University of Iowa
99 PUBLICATIONS **2,195** CITATIONS

SEE PROFILE

Environ. Sci. Technol. **2005**, *39,* 1214−1220

Development of Improved Materials for Environmental Applications: Nanocrystalline NaY Zeolites

WEIGUO SONG, GONGHU LI, VICKI H. GRASSIAN,* AND SARAH C. LARSEN*

Department of Chemistry, University of Iowa, Iowa City, Iowa 52242

Two nanocrystalline NaY samples were synthesized with Si/Al ratios of 1.8 and crystal sizes of 23 and 50 nm, respectively. The synthesized NaY zeolites were characterized by powder X-ray diffraction, scanning electron microscopy, nitrogen adsorption isotherms, silicon solid-state magic angle spinning NMR and FTIR spectroscopy. A commercial NaY sample was analogously characterized for comparison with the synthesized nanocrystalline NaY. FTIR spectroscopy of adsorbed pyridine was used to elucidate the adsorption sites on the different NaY samples. More Brønsted acid sites and more silanol sites were detected on the nanocrystalline NaY zeolites, relative to the commercial NaY. The nanocrystalline NaY exhibited increased adsorption capacities for representative pollutant molecules, such as toluene (∼10%) and nitrogen dioxide (∼30%), relative to commercial NaY. Functionalization of nanocrystalline NaY was examined as a method for tailoring the properties of nanocrystalline zeolites for specific environmental applications through the control of zeolite properties, such as hydrophobicity.

Introduction

Zeolites are crystalline aluminosilicates with pores of molecular dimensions that are widely used in applications, such as separations, catalysis, ion exchange, and adsorption (*1*−*4*). Zeolites are considered nanomaterials because of their pore sizes that range from approximately 0.4 to 1 nm. One of the first successful applications of nanotechnology was the use of zeolites as catalysts for industrial processes, such as petroleum refining (*5*). Recently, there has been a great deal of interest in another aspect of zeolites related to nanoscience, the primary crystal size, which can potentially be exploited for use in nanotechnology. Nanocrystalline zeolites are zeolites with discrete, uniform crystals with dimensions of less than 100 nm that have unique properties relative to conventional micrometer-sized zeolite crystals. Nanocrystalline zeolites have higher external surface areas and reduced diffusion path lengths relative to conventional micrometer-sized zeolites, which make them promising catalytic materials and adsorbents. For example, nanocrystalline ZSM-5 exhibits increased selectivity and toluene conversion into cresol and decreased coke formation relative to conventional ZSM-5 materials (*6*). Recently, it was shown that the adsorption capacity of nanocrystalline silicalite increased approximately 50% relative to micrometer-sized silicalite (*7*). In addition, nanometer-sized zeolites can be assembled into thin films and other porous nanoarchitectures for use as separation membranes (*8*), chemical sensors (*8*−*10*), and photochemical hosts (*11*, *12*).

Nanocrystalline zeolites have very large external surface areas (*7*, *13*). For zeolite crystals with sizes smaller than ∼30 nm, the external surface area is >100 m^2/g, the same order of magnitude as the internal surface area for a typical zeolite. Thus, the external surface of nanocrystalline zeolites can potentially be utilized for adsorption and catalytic reactions. In principle, a bifunctional material could be prepared from nanocrystalline zeolites, such that the external and internal surfaces have different reactivities. For example, the external surface active sites could catalyze the degradation reaction of a large molecule that could then diffuse into the zeolite pores for further reaction. The external surface could even be functionalized to vary the hydrophobicity/hydrophilicity of the zeolite. This is important for many applications, including the uptake of volatile organic compounds, such as toluene, from aqueous solutions. Natural zeolites, such as clinoptilolite, have been modified using surfactants and chlorosilanes in order to enhance the adsorption of aromatics from aqueous solutions (*14*, *15*). Similar strategies can be envisioned for nanocrystalline zeolites.

Zeolite Y is a faujasite molecular sieve with 7.4 Å diameter pores and a three-dimensional pore structure (*1*, *2*). The basic structural units for Y zeolites are the sodalite cages, which are arranged so as to form supercages that are large enough to accommodate spheres with 1.2 nm diameters. The primary application for Y zeolites has been in catalytic cracking of petroleum molecules into smaller gasoline range hydrocarbons (*2*). Recently, the synthesis of nanocrystalline zeolite Y has been reported by several groups (*11*, *16*−*19*). The nanocrystalline zeolite materials have been used as photochemical hosts in optically transparent solutions and to study zeolite crystal growth mechanisms (*11*, *12*, *16*).

In this paper, the synthesis, characterization, and adsorption properties of synthesized nanocrystalline zeolite Y are reported. The synthetic method used here is a modification of the method of Creaser and co-workers (*17*). The physicochemical properties of the synthesized, nanocrystalline NaY samples; the functionalization of the external surface of nanocrystalline NaY; and the potential of these materials for applications in environmental remediation are discussed.

Experimental Section

Materials. Aluminum isopropoxide, tetraethoxyorthosilane (TEOS), and sodium hydroxide were purchased from Alfa Aesar. Tetramethylammonium hydroxide (TMAOH) solution (25% wt) was purchased from Aldrich. All chemicals were used as purchased without further purification.

Nanocrystalline NaY Synthesis. Zeolite Y was synthesized using clear solutions according to the method reported by Creaser and co-workers (*17*). Aluminum isopropoxide, half of the TMAOH solution, and water were mixed and stirred until the mixture became a clear solution. Next, TEOS, the rest of the TMAOH solution, and water were added to the clear solution. The mixture was stirred overnight to ensure complete hydrolysis of the aluminum and silicon sources. The final clear synthesis gel had the following composition: 0.07 Na:2.4 TMAOH:1.0 Al:2.0 Si:132 H_2O:3.0 *i*-PrOH:8.0 EtOH; the latter two alcohols came from the hydrolysis of the aluminum isopropoxide and TEOS, respectively. To optimize the formation of small NaY crystals, the sodium content was

* Authors to whom correspondence should be addressed. Phone: (319)335-1346; fax: (319)335-1270; e-mail: sarah-larsen@uiowa.edu (S.C.L.); vicki-grassian@uiowa.edu (V.H.G.).

10.1021/es049194z CCC: $30.25
Published on Web 01/07/2005

intentionally set too low relative to aluminum content in the synthesis gel.

For sub-100-nm sized samples, the clear solution was transferred into a 500 mL flask equipped with an air cooled condenser and was heated to 95 °C in an oil bath for 84 h with (23 nm) or without stirring (50 nm). Nanocrystalline Y powders were recovered from the milky, colloidal suspension of NaY after two cycles of centrifugation, washed with deionized water, and dried at 120 °C in air. Nanocrystalline NaY samples were calcined at 500 °C under oxygen flow for 16 h to remove organic templates.

Functionalization of Nanocrystalline NaY. The external surface of NaY (23 nm) was functionalized following the procedure of Grassian and co-workers (*20*). Specifically, 0.2 g of calcined NaY was mixed with 100 mL of dry toluene, 0.4 mL of octylmethyldichlorosilane, and 0.2 mL of pyridine in a 250 mL flask equipped with a water-cooled condenser. The mixture was heated in an oil bath to 95 °C with stirring for 3 h. After being cooled, the solid powders were recovered by filtering and drying at 95 °C in an oven.

Elemental Analysis. A Perkin-Elmer plasma 400 inductively coupled plasma/atomic emission spectrometer (ICP/AES) spectrometer was used to determine the Si/Al ratio of the zeolite Y samples. NaY samples were acid digested by dilute HF solution followed by neutralization in $NaBO_3$. Four standard solutions with known silicon and aluminum concentrations were prepared as calibration standards. Atomic emission peak intensities at wavelengths of 309.2 nm for aluminum and 203.9 nm for silicon were recorded for all four standard solutions and the sample solution. Exact concentrations of aluminum and silicon in the sample solution were obtained by projection from the working curve generated from standard solution data.

Hitachi S-4000 Scanning Electron Microscope. To prepare the sample for SEM, a drop of dilute colloidal solution of the uncalcined sample was dropped onto the SEM sample stud surface, and the sample stud was then dried at 60 °C for 3 h. Shortly before acquiring an SEM image, the sample was coated with gold. From the SEM images, small NaY crystals are envisioned as cubic particles in order to estimate the particle size.

X-ray Diffraction. A Siemens D5000 X-ray diffractometer with Cu Kα target and nickel filter was used to collect XRD powder patterns for the samples. XRD patterns were collected between 2θ angles of 5 and 35°. The full-width at half-maximum (fwhm) of the peak from the slow scan of each sample was obtained by simulation and was used to estimate the crystal size of each NaY sample from Scherrer's equation (with $K = 1.0$) given below:

$$T = \frac{K\lambda}{\beta \cos \theta}$$

where T = crystal size (nm); K = crystal shape factor; λ = wavelength of X-rays (for Cu target, $\lambda = 1.542$ Å); β = fwhm; and θ = Bragg's angle.

Nitrogen Adsorption Isotherms. Nitrogen adsorption isotherms were obtained on a Quantachrome Nova 1200 multipoint BET apparatus using approximately 0.2 g of sample for each measurement. Immediately prior to the N_2 adsorption, each sample was vacuum degassed at 120 °C for 1 h. The specific surface area was measured by the BET method (*21*), which was performed automatically by the instrument. BET adsorption isotherms were collected for NaY samples before and after calcination to remove the template.

Solid State ^{29}Si NMR. ^{29}Si (59.6 MHz) solid-state magic angle spinning (MAS) NMR spectra were obtained using a 300 MHz wide bore magnet with a TecMag Discovery console and a Chemagnetics double-channel 7.5 mm pencil MAS probe with a spinning speed of ~6 kHz. Typically, 0.2 g of sample was used to load the rotor. Each single pulse spectrum was acquired by signal averaging 2000 scans with a 60 s pulse delay.

FTIR Spectroscopy. The sample cell used in the infrared study has been described previously (*22*). A total of 10 mg of Y zeolite was coated onto a 3×2 cm^2 photoetched tungsten grid held in place by nickel jaws. The nickel jaws are attached to copper leads so that the sample can be resistively heated. A thermocouple wire is used to measure the temperature of the sample. The tungsten grid with zeolite sample is placed inside of a stainless steel cube. The cube is outfitted with two BaF_2 windows for infrared measurements and is also attached to a vacuum/gas handling system. The IR cell is held in place by a linear translator inside the sample compartment of a Mattson Galaxy 6000 infrared spectrometer equipped with a narrowband MCT detector. Each spectrum was obtained by averaging 64 scans at an instrument resolution of 4 cm^{-1}. Zeolite samples were heated under vacuum at 400 °C overnight to remove adsorbed water prior to the FTIR measurements.

The NO_2 adsorption experiments were conducted at room temperature by equilibrating the zeolite with 500 mTorr NO_2 for 30 min and then pumping out the gas phase for several minutes before acquiring the FTIR spectra. In the pyridine adsorption experiment, the zeolite was first equilibrated with 1 Torr pressure of pyridine vapor at 200 °C for 30 min. It has been previously shown that desorption of weakly adsorbed pyridine takes place up to ~197 °C (*23*). The sample was then evacuated for 30 min and cooled to room temperature prior to recording FTIR spectra.

Adsorption of a Representative VOC. Toluene was selected as a representative volatile organic compound (VOC) to examine VOC adsorption as a function of the crystal size of NaY. The experimental setup has been described previously (*7*, *13*). Prior to each experiment, 0.1 g of calcined NaY sample was loaded into a 1/4 in. quartz tube. The sample bed was capped with quartz wool. The sample bed was heated at 400 °C under helium prior to the adsorption at room temperature. During room temperature adsorption, 25 standard cm^3/min of helium was directed through a toluene bubbler and then through the sample bed. After the sample was saturated with toluene, the toluene bubbler was bypassed to start purging the sample by helium flow at room temperature, and then the sampled was heated at 5 °C/min to do the TPD experiment. Throughout the experiment, the concentration of toluene in the gas stream was monitored by a thermal conductivity detector (TCD) detector of a Varian 3400CX gas chromatograph (GC), which was calibrated to give a quantitative measurement of the toluene concentration.

Results and Discussion

Synthesis and Characterization of Nanocrystalline NaY. The two nanocrystalline NaY samples with different average particles sizes of 23 and 50 nm were synthesized with (23 nm) and without (50 nm) stirring under otherwise identical conditions. The SEM images and XRD patterns of the two synthesized NaY samples and the commercial NaY (Aldrich) are shown in Figures 1 and 2, respectively. Close inspection of the SEM images indicates that the NaY (Aldrich) (Figure 1a) is composed of large intergrown NaY crystals with diameters of ~1−2 μm. The SEM images of the two synthesized nanocrystalline NaY samples indicate that the crystals are discrete with narrow size distributions and are substantially smaller than the NaY (Aldrich) crystals. The XRD patterns (Figure 2) agree with those for the faujasite structure of NaY (*24*). The line widths increase as the particle size decreases consistent with what is expected based on Scherrer's equation. The crystal sizes calculated from the XRD line widths and Scherrer's equation ($K = 1.0$) are listed in Table 1. Elemental analysis was performed using ICP/AES

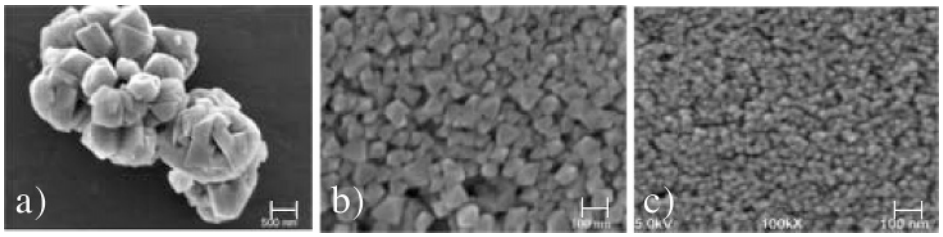

FIGURE 1. SEM images of three NaY samples: (a) NaY (Aldrich) (scale bar = 500 nm), (b) NaY (50 nm), and (c) NaY (23 nm). In panels b and c, the scale bar is equal to 100 nm.

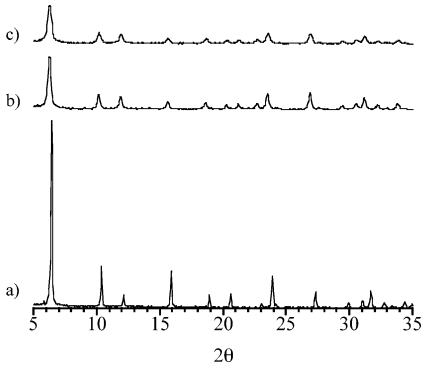

FIGURE 2. XRD patterns of NaY samples: (a) NaY (Aldrich), (b) NaY (50 nm), and (c) NaY (23 nm). 2θ angles between 5 and 55° were collected.

TABLE 1. Properties of Synthesized Nanocrystalline NaY Zeolites and Commercial NaY (Aldrich)

sample	Si/Al[a]	BET external surface area (m^2/g)[b,c]	BET total surface area (m^2/g)[c,d]	size from BET area (nm)[e]	size from XRD line width (nm)[f]
NaY (Aldrich)	2.0	na	477	na	53
NaY (50 nm)	1.8	81	510	50	19
NaY (23 nm)	1.8	178	584	23	14

[a] Si/Al was calculated from ICP/AES data. [b] BET measurement of as synthesized sample. [c] Standard deviations of surface areas were measured to be between 0.4 and 1.4 m^2/g; the larger errors are associated with the higher surface areas measured. [d] BET measurement of calcined sample. [e] Crystal size was obtained using the relationship, x (nm) = 4061/external surface area (m^2/g). [f] Crystal size obtained using Scherrer's equation (K = 1.0).

to determine the Si/Al ratio of the NaY samples. The Si/Al ratios (Table 1) were 2.0 for NaY (Aldrich) and 1.8 for the two synthesized samples.

Nitrogen adsorption isotherms for the synthesized NaY samples were measured both before (as-synthesized) and after calcination. The total surface areas of both calcined and as-synthesized samples were obtained from the nitrogen adsorption isotherms using the BET method and are listed in Table 1. The total surface area of the as-synthesized samples in which the internal surface is blocked by template molecules represents the external surface area of the zeolite sample. The total surface area obtained from the calcined samples contains contributions from both the internal and the external surfaces. The external surface areas for the as-synthesized NaY samples were 81 and 178 m^2/g with total surface areas of 510 and 584 m^2/g, respectively. For the NaY (Aldrich) sample, only the total surface area of 477 m^2/g was measured since the material was only available in the calcined form.

In previous work, we have demonstrated that the particle size can be accurately estimated using the external surface area if the crystals are assumed to be cubic (*7*, *13*). Using the external surface area measured from the BET method described above, the particle size can be estimated using the relationship below:

$$x = 4061/S_{ext}$$

where S_{ext} is the external surface area in m^2/g and x is the NaY particle size in nm (assuming cubic crystals). Using this relationship, the particle size was estimated from external surface area and is listed in Table 1. An analogous relationship was derived for nanocrystalline silicalite, and the experimentally determined external surface areas and particle sizes (from SEM) agreed remarkably well with the results of the calculation assuming cubic silicalite crystals (*7*, *13*). As determined in our previous work, the crystal sizes calculated from the XRD line widths reproduce the expected trend in crystal sizes; however, the sizes from the XRD line width are not quantitatively consistent with the SEM and BET results, and thus the measured line width is a poor method for estimating the particle size.

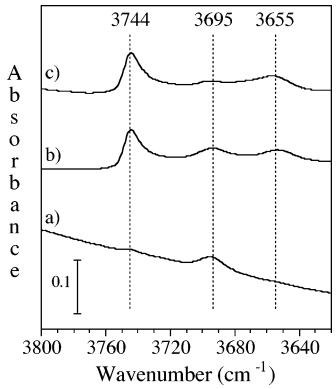

FIGURE 3. FTIR spectra of O−H stretching region for NaY samples: (a) NaY (Aldrich), (b) NaY (50 nm), and (c) NaY (23 nm).

Characterization of Nanocrystalline NaY by FTIR Spectroscopy. FTIR spectroscopy was used to identify structural features and adsorption sites in the NaY samples. The FTIR spectra of the O−H stretching region for all three NaY samples after thermal pretreatment at 400 °C under vacuum are shown in Figure 3 a−c. Three main peaks are observed at 3655, 3695, and 3744 cm^{-1}. The peaks at 3655 and 3695 cm^{-1} are assigned to O−H groups attached to extra framework alumina species and to O−H groups attached to Na^+ cations, respectively, based on a comparison with the literature (*25*, *26*). The peak at 3744 cm^{-1} is assigned to silanol groups (Si−OH) on NaY (*25*, *26*). The peaks at 3744 and 3695 are observed for all three samples, NaY (Aldrich), NaY (50 nm), and NaY (23 nm), although in different relative intensities. The silanol peak at 3744 cm^{-1} is weakest for NaY (Aldrich), relative to NaY (23 and 50 nm). The peak at 3655 cm^{-1} assigned to OH groups on extra framework alumina sites is only observed for NaY (50 nm) and NaY (23 nm), not for NaY (Aldrich).

The FTIR spectra of pyridine adsorbed on the NaY zeolites are shown in Figure 4 a−c. Pyridine molecules can adsorb and react at several different sites on the NaY zeolites. Pyridine

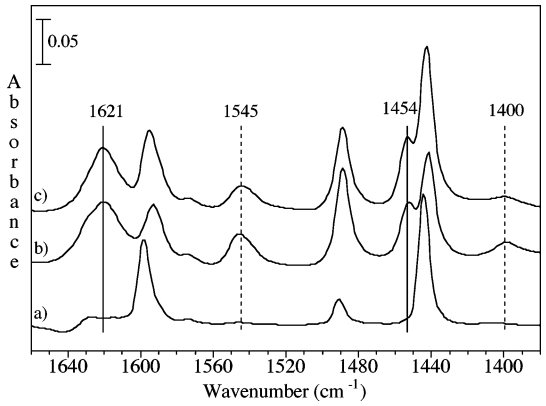

FIGURE 4. FTIR spectra of the adsorption of pyridine on (a) NaY (Aldrich), (b) NaY (50 nm), and (c) NaY (23 nm). The solid lines indicate peaks assigned to pyridine molecules adsorbed on Lewis acid sites, and the dashed lines are assigned to pyridine molecules adsorbed on Brønsted acid sites.

molecules can interact with Brønsted acid sites forming pyridinium ions, which are characterized by bands in the FTIR spectra at 1400 and 1545 cm^{-1} (*23*). The absorbances at 1621 and 1454 cm^{-1} are assigned to pyridine molecules adsorbed on Lewis acid sites (*23*). At the same time, pyridine molecules can physically adsorb via hydrogen bonding with surface hydroxyl groups, giving absorption bands at 1595, 1574, and 1443 cm^{-1} (*23*). All three interactions contribute to the band at 1489 cm^{-1}. Notable are the differences between the FTIR spectra of the NaY (Aldrich) sample and the NaY (23 and 50 nm) samples. The peaks at 1545 and 1400 cm^{-1} attributed to pyridine molecules on Brønsted acid sites are absent in the NaY (Aldrich) FTIR spectrum. In addition, the peaks assigned to pyridine adsorbed on Lewis acid sites are also very weak or absent in the FTIR spectrum of NaY (Aldrich).

The FTIR adsorption experiments described here provide insight into the different sites present in the NaY zeolites. Using the FTIR results, several key differences between the synthesized nanocrystalline NaY zeolites and the NaY (Aldrich) zeolite are highlighted. A greater number of extra framework alumina sites and Brønsted acid sites are detected on the nanocrystalline NaY samples relative to the NaY (Aldrich) sample. Since one of the major differences between these samples is the external surface area, it is possible that the extra framework alumina sites and the Brønsted acid sites are located on the external surface of the nanocrystalline zeolites. Further studies are in progress to address this issue of location of the extra framework alumina sites and the Brønsted acid sites.

Adsorption of a Representative VOC on NaY Zeolites. The adsorption of a typical VOC, toluene, on NaY was investigated using the flow apparatus described previously (*7*). Representative results from toluene adsorption/desorption on NaY samples are shown in Figure 5. The TCD signal of the GC is at a maximum when the sample bed is bypassed or when the sample is saturated and at a minimum when no toluene passes through the sample bed. In Region I of the experiment, toluene adsorption on the NaY sample was monitored. In Region II of the experiment, the NaY sample bed was purged with helium while monitoring the desorption of toluene, and in Region III of the experiment, a temperature-programmed desorption of the toluene was conducted. The amount of toluene adsorbed was obtained by measuring the area between the maximum baseline and the experimental curve, while the amount of toluene desorbed was obtained from the area between minimum baseline and the experimental curve profiles after the temperature ramp. Three experiments were run for each sample, and the average

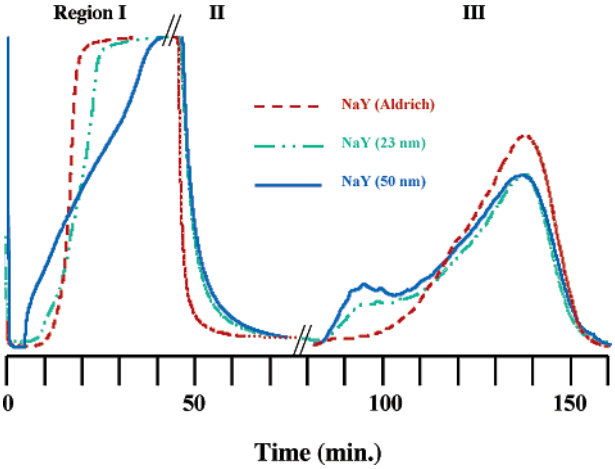

FIGURE 5. Toluene adsorption on nanocrystalline NaY (50 and 23 nm) and NaY (Aldrich). Each experiment consists of three regions: Region I, room temperature adsorption; Region II, room temperature purge with helium; and Region III, temperature-programmed desorption (TPD). Blue solid line, NaY (23 nm); green dotted line, NaY (50 nm); and red dashed line, NaY (Aldrich).

TABLE 2. Toluene Adsorption and Desorption on NaY Samples[a]

sample	adsorption (mmol/g)	purge (mmol/g)	TPD (mmol/g)	total desorption (mmol/g)
NaY (Aldrich)	2.08 (0.08)	0.21 (0.01)	1.95 (0.04)	2.16 (0.05)
NaY (50 nm)	2.19 (0.03)	0.40 (0.02)	1.86 (0.08)	2.26 (0.10)
NaY (23 nm)	2.34 (0.04)	0.45 (0.01)	1.92 (0.04)	2.37 (0.05)

[a] Data listed are the average of three runs for each sample. Standard deviations are in parentheses.

amounts of toluene adsorbed and desorbed in this experiment were calculated and are listed in Table 2.

The total toluene adsorption in Region I of the experiment was 2.08, 2.19, and 2.34 mmol/g for NaY (Aldrich), NaY (50 nm), and NaY (23 nm), respectively. The total toluene adsorption trends with total surface area. The amount of toluene removed during the helium purge was 0.21 mmol/g for NaY (Aldrich), 0.40 mmol/g for NaY (50 nm), and 0.45 mmol/g for NaY (23 nm). The area under the desorption peaks in Region III of the experiment is approximately the same for all three samples and ranges from 1.86 to 1.95 mmol/g. However, while the area of the TPD peak is approximately the same for all three samples, the shape of the TPD peak is different for the different samples. The TPD peaks for NaY (23 and 50 nm) have two maxima, suggesting that the toluene is adsorbed at two different sites in the zeolite. However, the TPD peak for NaY (Aldrich) only has the higher temperature desorption component.

Previously, for analogous toluene adsorption/desorption experiments on silicalite and ZSM-5, the total toluene adsorption trended linearly with total surface area (*7*, *13*). For the results reported here, the toluene adsorption on NaY samples in Region I also trends linearly with the total surface area. In the earlier work, the toluene desorbed during the helium purge (Region II) was attributed to weakly bound toluene on the external surface of silicalite and ZSM-5 samples based on a strong correlation between the external surface area and the amount of toluene desorbed during the helium purge. This strong correlation between external surface area and weakly adsorbed toluene does not hold for the NaY samples used in this study. The amount of toluene desorbed in Region II is approximately the same for NaY (23 nm) and NaY (50 nm) despite the fact that the external surface area for NaY (23 nm) is twice as large as the external surface area

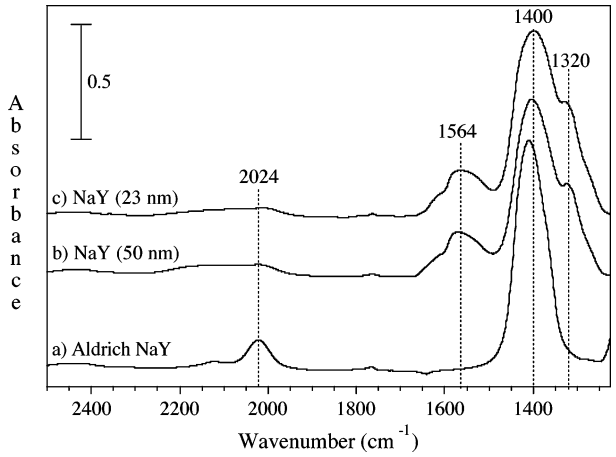

FIGURE 6. FTIR spectra of NO_2 adsorption on (a) NaY (Aldrich), (b) NaY (50 nm), and (c) NaY (23 nm).

for NaY (50 nm). The external surface area for NaY (Aldrich) was not measured but is estimated to be <10 m^2/g, consistent with the small amount of toluene adsorbed on the external surface. The amount of toluene desorbed during the TPD experiment is approximately the same for all of the samples, but NaY (23 and 50 nm) data indicate that some of the toluene is more weakly adsorbed as evidenced by the low temperature desorption feature. The significantly lower Si/Al ratios of the Y zeolites discussed here relative to the silicalite (purely siliceous) and ZSM-5 (Si/Al = 20) should be noted since it will impact the adsorption sites for toluene.

These adsorption/desorption results indicate that the overall adsorption capacity of nanocrystalline NaY is approximately 10% greater than the NaY (Aldrich) largely due to the higher external surface area and the weakly adsorbed toluene that desorbs during the room temperature helium purge of the sample. The strongly adsorbed toluene that desorbs during the temperature-programmed desorption is quantitatively similar for all of the NaY samples, although two desorption peaks are observed for the nanocrystalline NaY samples.

Adsorption of an Atmospheric Pollutant on NaY. The emission of NO_x from stationary and automotive sources, such as power plants and lean-burn engines, is a major environmental pollution issue. NO_x leads to the production of ground-level ozone and acid rain. The adsorption and catalytic reduction of nitrogen oxides to N_2 are important environmental challenges for scientists and engineers. The adsorption of NO_2 on NaY was investigated using FTIR spectroscopy. Figure 6a−c shows the difference FTIR spectra of NO_2 adsorption in all three NaY samples. Spectral features observed can be identified as NO^+ (2000−2180 cm^{-1} spectral region) and NO_3^- (1300−1600 cm^{-1} spectral region) (*25*−*29*). The NO^+ and NO_3^- species are proposed to form through a cooperative effect whereby two adsorbed NO_2 molecules in close proximity autoionize according to the reaction (*27*):

$$(NO_2)_2 \rightarrow NO^+ + NO_3^- \quad (1)$$

A second minor pathway has recently been proposed (*27*) in which strongly bound H_2O in NaY reacts with NO_2 to from nitric acid and nitrous acid (HONO) according to the reaction below (*30*−*33*):

$$2NO_2 + H_2O \rightarrow HNO_3 + HONO \quad (2)$$

The nitric acid readily reacts with Na^+ cations in NaY zeolites to form $Na^+NO_3^-$ and a Brønsted acid site. The Brønsted acid site can then react with NO_2 to form NO^+ and water. In accord with previous assignments in the literature, the band at ~1400 cm^{-1} is assigned to NO_3^- adsorbed on Na^+ cation site in NaY (*27*, *32*), and the band at 2024 cm^{-1} is assigned to NO^+ adsorbed on Lewis base sites. The bands at ~1564 and 1320 cm^{-1} are assigned to NO_3^- adsorbed on extra framework alumina sites (*26*, *27*).

Clear differences are observed in the spectra of NO_2 adsorbed on NaY (Aldrich) as compared to NO_2 adsorbed on NaY(23 nm) and NaY (50 nm). Two prominent peaks are observed at 1564 and 1320 cm^{-1} in the FTIR spectra of NO_2 adsorbed on NaY (23 nm) and NaY (50 nm) (Figure 4b,c). These two peaks are absent in the FTIR spectrum of NO_2 adsorbed on NaY (Aldrich) (Figure 4a). This is consistent with the FTIR spectra of the hydroxyl group region shown in Figure 3, which indicated that extra framework alumina sites were present on NaY (23 nm) and NaY (50 nm) but not on NaY (Aldrich).

Quantitative information about the relative adsorption capacities of these zeolites can also be obtained from the FTIR data. Using volumetric methods, the adsorption capacities for NO_2 on NaY (Aldrich), NaY (50 nm), and NaY (23 nm) were measured and were determined to be 1.23, 1.42, and 1.68 mmol/g, respectively. This represents a 30% increase in adsorption capacity for NaY (23 nm) relative to NaY (Aldrich). Work is in progress to determine the effectiveness of nanocrystalline NaY for the selective catalytic reduction of NO_x with hydrocarbons.

Functionalization of Nanocrystalline NaY for Environmental Applications. The ability to tailor the properties of nanocrystalline zeolites for specific environmental applications is an important issue. For example, nanocrystalline zeolites can be functionalized using chlorosilane reagents to change the hydrophobic/hydrophilic properties of the zeolites. This is beneficial for applications in which pollutants present in solvents with different properties must be removed. This idea can be extended to include the development of bifunctional zeolites based on the introduction of different functionalities on the external and internal surfaces of the nanocrystalline zeolites. In this way, a pollutant molecule that is too large to fit inside the zeolite pores could react on the external surface and the products could then diffuse into the pores for further reaction or degradation of the pollutant.

NaY can be functionalized through reaction of the zeolite silanol groups (Si−OH) with a chlorosilane reagent (*34*−*36*). The silanol groups are located on the external surface as discussed previously in the literature (*37*) and supported by the FTIR results presented here that show that nanocrystalline NaY contains substantially more silanol groups than Aldrich NaY. In this work, octamethyldichlorosilane was used as the chlorosilane reagent designed to react with the silanol groups of NaY (23 nm) according to the following reactions (*20*):

$$\equiv Si{-}OH + CH_3(CH_2)_7SiCH_3Cl_2 \rightarrow \equiv Si{-}O{-}Si{-}(CH_3)(Cl)(CH_2)_7CH_3 + HCl \quad (3)$$

$$\equiv Si{-}OH + \equiv Si{-}O{-}Si{-}(CH_3)(Cl)(CH_2)_7CH_3 \rightarrow (\equiv Si{-}O)_2{-}Si{-}(CH_3)(CH_2){-}CH_3 + HCl \quad (4)$$

To confirm the functionalization of the silanol groups, FTIR spectroscopy and ^{29}Si MAS NMR spectroscopy were used. The O−H stretching region of the FTIR spectrum (not shown) of the functionalized NaY (23 nm) indicated the complete loss of silanol groups. The ^{29}Si MAS NMR spectra of the calcined NaY (23 nm) sample is shown in Figure 7a. Peaks in the spectral region from approximately −80 to −120 ppm are observed and can be assigned to silicate species in the zeolite framework. Q^3 and Q^4 silicate signals are observed where the Q^n nomenclature is used, such that n represents the number of siloxane bonds and $(4-n)$ provides the number of silanol (Si−OH) groups. When the NaY (23 nm) sample

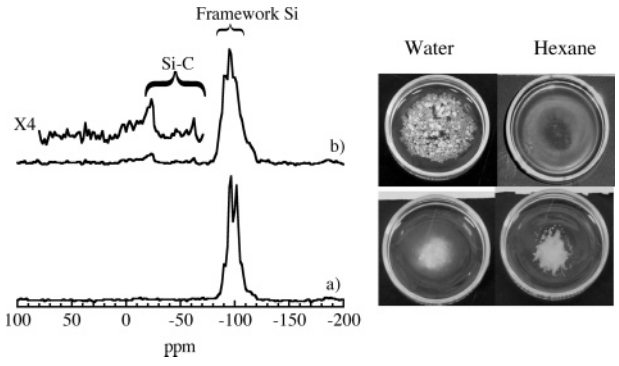

FIGURE 7. ^{29}Si MAS NMR spectra of (a) calcined NaY (23 nm) and (b) NaY (23 nm) functionalized with octylmethyldichlorosilane. Digital images of the functionalized and the parent NaY in different solvents are shown on the right-hand side of the figure. Images of the functionalized NaY mixed with water and hexane, respectively, are shown in the top row from left to right. Images of the parent NaY mixed with water and hexane, respectively are shown in the bottom row from left to right.

was functionalized with octamethyldichlorosilane, new peaks at ∼−62 and −23 ppm are observed in the ^{29}Si MAS NMR spectrum (Figure 7b). Peaks in the range of 10 to −70 ppm are typically attributed to ^{29}Si resonances of organosilane compounds (*35*, *36*, *38*). Consequently, these peaks are assigned to the two functionalized Si groups depicted in reactions 3 and 4 (*35*). Based on similar assignments in the literature, the peak at −23 ppm is assigned to the monochloro species in reaction 3 (*36*, *38*−*41*). The peak at −62 ppm is assigned to the organosilane surface species depicted in reaction 4 (*38*). The functionalization of NaY (Aldrich) was also attempted, but the functionalization of the Si−OH groups was not detected by ^{29}Si MAS NMR. Presumably, this is due to the low sensitivity of the ^{29}Si NMR experiment because of the relatively small number of silanol groups (Figure 3) available for functionalization.

Through functionalization of the zeolite framework with an octamethyl hydrocarbon chain, the hydrophobicity of the NaY is dramatically increased. A visual demonstration is illustrated using digital camera images shown on the right side of Figure 7. The increased hydrophobicity is illustrated by a visual comparison of functionalized NaY (23 nm) mixed with water (top left) and hexane (top right). When functionalized NaY (23 nm) is mixed with water, the zeolite repels the water to the extent that it aggregates and floats on the surface of the water. This is in contrast to the uniform mixing that was observed with hexane as a solvent. For comparison, analogous images of the parent NaY (23 nm) in water and hexane are shown in Figure 7 directly below the images for the functionalized NaY (23 nm). The parent NaY (23 nm) mixes uniformly with both water and hexane.

Future Applications for Nanocrystalline Zeolites in Environmental Applications. Zeolites have emerged as important materials for environmental applications, such as emission abatement of nitrogen oxides, environmentally benign synthesis, and adsorption of VOC's and other pollutants (*42*). Nanocrystalline zeolites have several advantages relative to conventional zeolites that may enhance their usefulness for environmental applications. The increased surface area of nanocrystalline zeolites relative to commercial zeolites is one advantage that can be exploited for applications of zeolites as adsorbents of VOCs and other pollutants. The increase in adsorption capacity of the nanocrystalline zeolites for toluene relative to commercial zeolites ranges from 15 to 50% depending on the parent zeolite and the size of the nanocrystalline material (*7*, *13*). Nitrogen dioxide adsorption on nanocrystalline NaY (23 nm) was increased by ∼30% relative to NaY (Aldrich). Future work in this area will focus on characterizing the different adsorption sites on the internal and external surfaces of the nanocrystalline zeolites so that these materials can be tailored for specific applications.

Another potential application for nanocrystalline zeolites is in environmental catalysis. Environmental catalysis involves the use of catalysts to solve environmental problems, in areas such as emission abatement and environmentally benign synthesis (*42*−*44*). Many new catalysts and catalytic processes have been developed to meet the challenges posed by environmental concerns. Besides emissions abatement, the emphasis of environmental catalysis has expanded to include the development of environmentally benign synthetic routes designed to decrease the amount of chemical waste produced. Recently, zeolites have emerged as important materials for applications in environmental catalysis, such as emission abatement of nitrogen oxides and environmentally benign synthesis (*4*, *43*−*45*). The selective catalytic reduction of NO_x and N_2O by hydrocarbons (HC−SCR) over zeolites, particularly in the presence of oxygen, has attracted much interest for emission abatement applications in stationary sources, such as natural gas fueled power plants (*26*, *27*, *43*, *46*−*48*). HC−SCR of NO_x shows promise for applications to lean-burn gasoline and diesel engines where noble-metal three-way catalysts are not effective at reducing NO_x in the presence of excess oxygen. Work is in progress to evaluate nanocrystalline zeolites for applications in environmental catalysis.

Acknowledgments

The research described in this paper has been funded by the Environmental Protection Agency through EPA Grant R82960001 to S.C.L. and V.H.G.

Literature Cited

(1) Breck, D. W. *Zeolite Molecular Sieves*: *Structure, Chemistry, and Use*; Wiley-Interscience: New York, 1974.
(2) Gates, B. C. *Catalytic Chemistry*; Wiley: New York, 1992.
(3) Corma, A. State of the art and future challenges of zeolites as catalysts. *J. Catal.* **2003**, *216*, 298−312.
(4) Marcus, B. K.; Cormier, W. E. Going green with zeolites. *Chem. Eng. Prog.* **1999**, 47−53.
(5) Ratner, M.; Ratner, D. *Nanotechnology*: *A Gentle Introduction to the Next Big Idea*; Prentice Hall: Upper Saddle River, NJ, 2003.
(6) Vogel, B.; Schneider, C.; Klemm, E. The synthesis of cresol from toluene and N_2O on H[Al]ZSM-5: Minimizing the product diffusion limitation by the use of small crystals. *Catal. Lett.* **2002**, *79*, 107−112.
(7) Song, W.; Justice, R. E.; Jones, C. A.; Grassian, V. H.; Larsen, S. C. Size-dependent properties of nanocrystalline silicalite synthesized with systematically varied crystal sizes. *Langmuir* **2004**, *20*, 4696−4702.
(8) Bein, T. Synthesis and applications of molecular sieve layers and membranes. *Chem. Mater.* **1996**, *8*, 1636−1653.
(9) Meinershagen, J. L.; Bein, T. Optical sensing in nanopores. encapsulation of the solvatochromic dye nile red in zeolites. *J. Am. Chem. Soc.* **1999**, *121*, 448−449.
(10) Mintova, S.; Bein, T. Nanosized zeolite films for vapor-sensing applications. *Microporous Mesoporous Mater.* **2001**, *50*, 159−166.
(11) Castagnola, N. B.; Dutta, P. K. Spectroscopic studies of colloidal solutions of nanocrystalline $Ru(bpy)_3^{2+}$-zeolite Y. *J. Phys. Chem. B* **2001**, *105*, 1537−1542.
(12) Castagnola, N. B.; Dutta, P. K. Nanometer-sized zeolite X crystals: Use as photochemical hosts. *J. Phys. Chem. B* **1998**, *102*, 1696−1702.
(13) Song, W.; Justice, R. E.; Jones, C. A.; Grassian, V. H.; Larsen, S. C. Synthesis, characterization and adsorption properties of nanocrystalline ZSM-5. *Langmuir* **2004**, *20*, 8301−8306.
(14) Bowman, R. S. Applications of surfactant modified zeolites to environmental remediation. *Microporous Mesoporous Mater.* **2003**, *61*, 43−56.
(15) Huttenloch, P.; Roehl, K.; Czurda, K. Sorption of nonpolar aromatic contaminants by chlorosilane surface modified natural minerals. *Environ. Sci. Technol.* **2001**, *35*, 4260−4264.

(16) Mintova, S.; Olsen, N. H.; Bein, T. Electron microscopy reveals the nucleation mechanism of zeolite Y from precursor colloids. *Angew. Chem., Int. Ed.* **1999**, *38*, 3201−3204.
(17) Li, Q.; Creaser, D.; Sterte, J. An investigation of the nucleation/crystallization kinetics of nanosized colloidal faujasite zeolites. *Chem. Mater.* **2002**, *14*, 1319−1324.
(18) Holmberg, B. A.; Wang, H.; Norbeck, J. M.; Yan, Y. Controlling size and yield of zeolite Y nanocrystals using tetramethylammonium bromide. *Microporous Mesoporous Mater.* **2003**, *59*, 13−28.
(19) Zhu, G.; Qiu, S.; Yu, J.; Sakamoto, Y.; Xiao, F.; Xu, R.; Terasaki, O. Synthesis and characterization of high-quality zeolite LTA and FAU single nanocrystals. *Chem. Mater.* **1998**, *10*, 1483−1486.
(20) Usher, C. R.; Michel, A. E.; D., S.; Grassian, V. H. Laboratory studies of ozone uptake on processed mineral dust. *Atmos. Environ.* **2003**, *37*, 5337−5347.
(21) Sing, K. S. W.; Everett, D. H.; Haul, R. A.; Moscou, L.; Pierotti, R. A.; Rouquerel, J.; Siemieniewsha, T. Reporting physisorption data for gas solid systems with special reference to the determination of surface-area and porosity. *Pure Appl. Chem.* **1985**, *57*, 603−619.
(22) Li, G.; Xu, M.; Larsen, S. C.; Grassian, V. H. Photooxidation of cyclohexane and cyclohexene in BaY. *J. Mol. Catal. A* **2003**, *194*, 169−180.
(23) Basila, M. R.; Kantner, T. R.; Rhee, K. H. The nature of the acidic sites on a silica−alumina. Characterization by infrared spectroscopic studies of trimethylamine and pyridine chemisorption. *J. Phys. Chem.* **1964**, *68*, 3197−3207.
(24) Meier, W. M.; Olson, D. H. *Atlas of Zeolite Structure*, 2nd revised ed.; Butterworth: Cambridge, 1987.
(25) Angell, C. L.; Schaffer, P. C. Infrared spectroscopic investigations of zeolites and adsorbed molecules. I. Structural OH groups. *J. Phys. Chem.* **1965**, *69*, 3463−3470.
(26) Sedlmair, C.; Gil, B.; Seshan, K.; Jentys, A.; Lercher, J. A. An in situ IR study of the NOx adsorption/reduction mechanism on modified Y zeolites. *Phys. Chem. Chem. Phys.* **2003**, *5*, 1897−1905.
(27) Szanyi, J.; Kwak, J. H.; Moline, R. A.; Peden, C. H. F. The adsorption of NO_2 and the $NO+O_2$ reacion on NaY, FAU: An in situ FTIR investigation. *Phys. Chem. Chem. Phys.* **2003**, *5*, 4045−4051.
(28) Chao, C.; Lunsford, J. H. Adsorption of nitric oxide on Y-type zeolites. A low-temperature infrared study. *J. Am. Chem. Soc.* **1971**, *93*, 6794−6800.
(29) Chao, C.; Lunsford, J. H. Infrared studies of the disproportionation reaction of nitric oxide on Y-type zeolites. *J. Am. Chem. Soc.* **1971**, *93*, 71−77.
(30) Borensen, C.; Kirchner, U.; Scheer, V.; Vogt, R.; Zellner, R. Mechanism and kinetics of the reactions of NO_2 or HNO_3 with alumina as a mineral dust model compound. *J. Phys. Chem. A* **2000**, *104*, 5036−5045.
(31) Goodman, A. L.; Underwood, G. M.; Grassian, V. H. A spectroscopic investigation of the heterogeneous reaction $2NO_2 + H_2O(a)$ $HONO(g) + HNO_3(a)$ on hydrated silica particles: Characterization of gas-phase and adsorbed products. *J. Phys. Chem. A* **1999**, *103*, 7217−7223.
(32) Goodman, A. L.; Miller, T. M.; Grassian, V. H. Heterogeneous reactions of nitrogen dioxide on Al_2O_3 and NaCl particles. *J. Vac. Sci. Technol. A* **1998**, *16*, 2585−2590.
(33) Saliba, N. A.; Yang, H.; Finlayson-Pitts, B. J. Reaction of gaseous nitric oxide with nitric acid on silica surfaces in the presence of water at room temperature. *J. Phys. Chem. A* **2001**, *105*, 10339−10346.
(34) Ding, W.; Meitzner, G. D.; Iglesia, E. The effects of silanation of external acid sites on the structure and catalytic behavior of Mo/H-ZSM-5. *J. Catal.* **2002**, *206*, 14−22.
(35) Song, W.; Marcus, D. M.; Abubakar, S. M.; Jani, E.; Haw, J. F. Trimethylsilation of framework Bronsted acid sites in microporous zeolites and silico-aluminophosphates. *J. Am. Chem. Soc.* **2003**, *125*, 13964−13965.
(36) Zhan, B.-Z.; White, M. A.; Lumsden, M. Bonding of organic amino, vinyl, and acryl groups to nanometer-sized NaX zeolite crystal surfaces. *Langmuir* **2003**, *19*, 4205−4210.
(37) Pu, S.-B.; Inui, T. Diffuse reflectance i.r. spectroscopic study on hydroxyl groups of H-ZSM-5s having different sizes and properties. *Zeolites* **1997**, *19*, 452−454.
(38) Sindorf, D. W.; Maciel, G. E. Solid-state NMR studies of the reactions of silica surfaces with polyfunctional chloromethylsilanes and ethoxymethylsilanes. *J. Am. Chem. Soc.* **1983**, *105*, 3767−3776.
(39) Mann, S.; Burkett, S. L.; Davis, S. A.; Fowler, C. E.; Mendelson, N. H.; Sims, S. M.; Walsh, D.; Whilton, N. T. Sol−gel synthesis of organized matter. *Chem. Mater.* **1997**, *9*, 2300−2310.
(40) De Paul, S. M.; Zwanziger, J. W.; Ulrich, R.; wiesner, U.; Spiess, H. W. Structure, mobility and interface characterization of self-organized organic−inorganic hybrid materials by solid-state NMR. *J. Am. Chem. Soc.* **1999**, *121*, 5727−5736.
(41) Wirth, M. J.; Fairbank, R. W. P.; Fatunmbi, H. O. Mixed self-assembled monolayers in chemical separations. *Science* **1997**, *275*, 44−47.
(42) Larsen, S. C. In *Environmental Catalysis*; Grassian, V. H., Ed.; CRC Press: Boca Raton, FL, 2005.
(43) Armor, J. N. Environmental catalysis. *Appl. Catal. B* **1992**, *1*, 221−256.
(44) Centi, G.; Ciambelli, P.; Perathoner, S.; Russo, P. Environmental catalysis: Trends and outlook. *Catal. Today* **2002**, *75*, 3−15.
(45) Masciangioli, T.; Zhang, W.-X. Environmental technologies at the nanoscale. *Environ. Sci.Technol.* **2003**, *37*, 102A−108A.
(46) Armor, J. N. Catalytic solutions to reduce pollutants. *Catal. Today* **1997**, *38*, 163−167.
(47) Long, R. Q.; Yang, R. T. Superior Fe-ZSM-5 catalyst for the selective catalytic reduction of nitric oxide by ammonia. *J. Am. Chem. Soc.* **1999**, *121*, 5595−5596.
(48) Long, R. Q.; Yang, R. T. Catalytic Performance of Fe-ZSM-5 catalysts for the selective catalytic reduction of nitric oxide by ammonia. *J. Catal.* **1999**, *188*, 332−339.

Received for review May 31, 2004. Revised manuscript received September 28, 2004. Accepted October 19, 2004.

ES049194Z